Double *K*-shell ionization probability in ^{54}Mn

M. M. Hindi,* C. A. White,† and R. L. Kozub
Department of Physics, Tennessee Technological University, Cookeville, Tennessee 38505, USA
(Received 23 July 2002; published 25 July 2003)

We have measured the probability of double *K*-shell vacancy production in the electron capture decay of ^{54}Mn to the 835-keV level of ^{54}Cr. The probability was deduced from the number of triple coincidences among the Cr hypersatellite and satellite x rays emitted in filling the double vacancy and the 835-keV γ ray. The probability of double *K*-shell vacancy production per *K*-shell electron capture (P_{KK}) was found to be $(2.3^{+0.8}_{-0.5})\times 10^{-4}$. Comparisons to previous experimental results and theoretical calculations are discussed.

DOI: 10.1103/PhysRevC.68.014306 PACS number(s): 23.40.−s, 23.90.+w, 27.40.+z, 32.80.Hd

I. INTRODUCTION

Double *K*-shell ionization accompanying electron capture (EC) is a process in which the sudden change of potential associated with *K* EC causes the remaining *K* electron to be ejected from the atom (shakeoff) or promoted to unoccupied levels (shakeup). The probability of the process is very sensitive to the electron-electron correlations in the atomic wave function. Because of the small probability (P_{KK}) with which the process takes place, ($\sim 10^{-4}$–10^{-5}) the measurements are difficult and susceptible to error. P_{KK} has been measured for only about 15 isotopes, most of which involve ground state to ground state EC transitions [1]. More often than not, the measurements on the same isotope are in conflict, sometimes by an order of magnitude or more. The theoretical situation is not settled either.

The predictions of the two leading theories [2,3] differ from each other by almost an order of magnitude at high *Z*. The data fall in between the two theories and do not clearly favor one against the other. Although the two theories diverge with *Z*, both predict a smooth decrease of P_{KK} with *Z* for decays with *Q* value much higher than the *K*-shell binding energy. The measured values of P_{KK} for ^{65}Zn [4] and ^{54}Mn [5] are both higher, by almost a factor of 3, than that of the neighboring (in atomic number) ^{55}Fe [6] and hence seem to be anomalously high. For both of these isotopes, the EC decay is to an excited state that decays promptly via γ emission. It is possible that the fluorescence caused by the γ rays in those decays increases the background on the high-energy side of the hypersatellite peak, thus distorting the peak shape used in the fit. We have remeasured P_{KK} for ^{54}Mn to double check its seemingly anomalously high value. In our measurement, the 835-keV γ ray was detected in triple coincidence with the satellite and hypersatellite *K* x rays in order to eliminate the possibility of fluorescence caused by the γ ray.

II. EXPERIMENTAL PROCEDURES

A. Source preparation

A thin source of 0.27 μCi strength was prepared by evaporating several drops of a solution of $MnCl_2$ in 1.0*M* HCl on a piece of scotch tape. The source was sandwiched between two HPGe detectors, one a coaxial detector with a 44 mm diameter, 49 mm depth, and a 0.5-mm-thick Be window, and the other a planar detector with a 16 mm diameter, 10 mm depth, and a 0.128-mm-thick Be window. The coaxial detector was used to detect the 835-keV γ ray emitted by the ^{54}Cr daughter and the planar detector was used to detect the Cr "normal" K^N x rays that are emitted after a single vacancy is created in the *K* shell following EC, as well as the *sum* (K^S+K^H) of the satellite and hypersatellite x rays that are emitted when a double vacancy is created in the *K* shell.

B. Measurements

The detectors were connected to amplifiers equipped with pileup rejection circuitry. For the x-ray detector two amplifiers were used, one with a shaping time of 10 μs and another with a shaping time of 0.25 μs. The combination was used to further reduce the pileup of $K+K$ signals in the x-ray detector (as explained below). A standard circuit was used to generate coincidence signals. The energy and timing signals were digitized in a four-channel analog-to-digital converter in a CAMAC crate interfaced to a PC running Linux. The digitized signals were recorded event by event on a magnetic tape using a locally written data acquisition software. Most of the recorded data consisted of double coincidences only, with singles runs collected for short periods of time every few days. The total data collection time was 130 days.

Figure 1 shows a sample singles spectrum recorded in the coaxial detector. Apart from a small ^{60}Co contamination in the source (which was purchased from Oxford Instruments), the spectrum is dominated by the 835-keV line. The x-ray spectra used in extracting P_{KK} were obtained by first setting a gate on the 835-keV line in the coaxial detector.

To reduce the pileup of $K+K$ signals, a gate was set on a two-dimensional (2D) histogram of the x-ray signal recorded with the short-time-constant amplifier (E_{short}) vs the signal recorded with the long-time-constant amplifier (E_{long}). Fig-

*Present address: Lockheed Martin Advanced Technology Center, 3251 Hanover Street, Palo Alto, CA 94304.
†Present address: MS-23, The University of Tennessee Space Institute, B. H. Goethert Parkway, Tullahoma, TN 37388-9700.

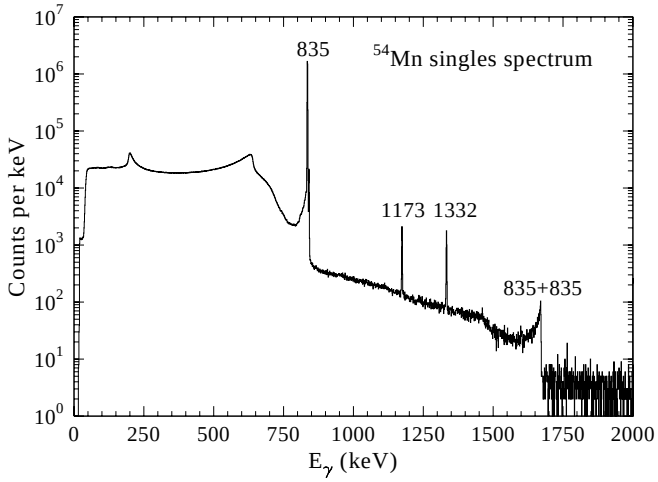

FIG. 1. A singles spectrum of the ^{54}Mn source, recorded with the coaxial Ge detector. The line energies are given in keV.

ure 2 shows a sample spectrum of E_{short} vs E_{long}. As expected, this spectrum shows that the pileup pulses that give an amplitude larger than that of the K peaks in E_{long} give an amplitude that is almost equal to that of the K peaks in E_{short}. Hence, a further improvement in the pileup rejection (over that of the hardware circuitry of the long-time-constant amplifier, already applied to the signals histogrammed in Fig. 2) can be achieved by placing a 2D gate around the $E_{\text{short}} = E_{\text{long}}$ locus. This additional pileup rejection is obtained without sacrificing the good energy resolution obtained with the long-time-constant amplifier.

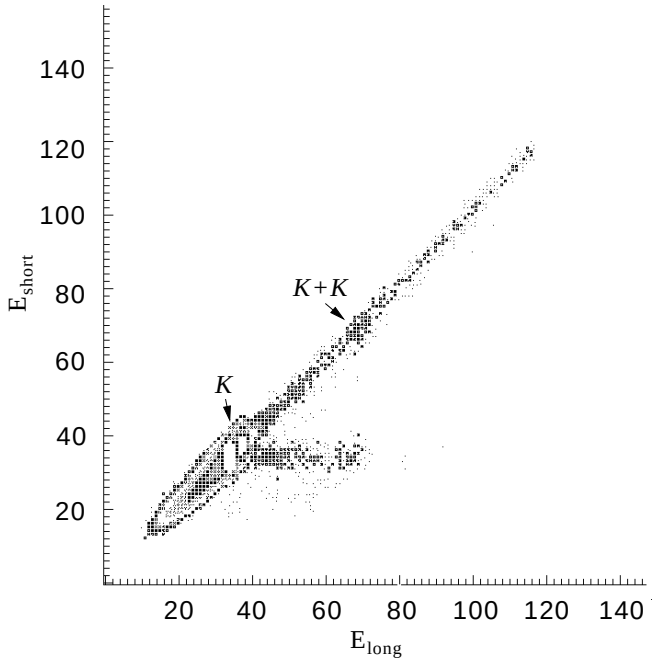

FIG. 2. Two-dimensional density plot of events as a function of x-ray energy recorded with the long-time-constant amplifier (E_{long}) and the short-time-constant amplifier (E_{long}). The spectrum is gated by the 835-keV line.

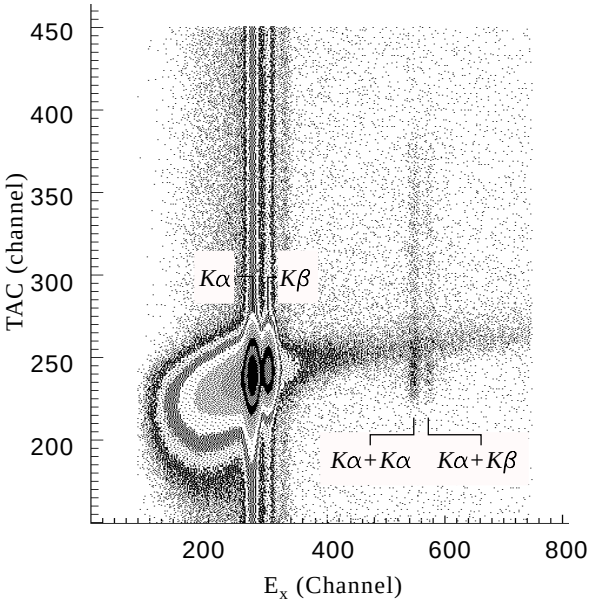

FIG. 3. Two-dimensional density plot of events as a function of the TAC signal between the γ- and x-ray detectors (y axis) and the energy recorded in the x-ray detector with the long-time-constant amplifier (x axis). The spectrum is gated by the 835-keV line.

Further reduction in the pileup can be achieved by setting an energy-specific gate on the time-to-amplitude (TAC) signal. Figure 3 shows a 2D histogram (gated by the 835-keV line and by the E_{short} vs E_{long} gate) of the TAC signal vs the energy in the x-ray detector (E_{long}). We use the leading-edge method to derive the fast timing signals. As a result, the TAC signal is amplitude (i.e., energy) dependent. In our setup, the TAC is started on the x-ray detector and stopped on the γ detector. The small-amplitude signals in the x-ray detector reach the leading-edge threshold at a later time and hence start the TAC later, thus leading to a smaller TAC signal. Conversely, large-amplitude signals reach the leading-edge threshold earlier and hence start the TAC earlier, thus leading to a larger TAC signal. This explains the increase in the TAC amplitude with energy in Fig. 3. The TAC spectrum in the region of the $K+K$ sum has a component that is lower than the expected TAC signal for that energy, and is characteristic of the TAC signal for a single K energy. Clearly, these TAC signals are from the pileup pulses where the time signal is picked off the first K x ray that enters the detector. The TAC spectrum in the region of the $K+K$ sum also shows accidentals (on the long-time side) that drop sharply about 240 ns from the prompt peak (channel ~380 in Fig. 3). These accidental signals arise from the x-ray detector triggering on a K x ray, with the corresponding 835-keV γ ray escaping detection, followed by another decay where both the x ray and the γ ray are detected, each in its own detector, thus leading to a signal in the $K+K$ region in the x-ray detector. If the second decay happens later than 240 ns after the first, the x-ray signals will fall outside of the E_{short} vs E_{long} gate (or, if later than about 400 ns, then they are rejected by the pileup rejector in the amplifier), and hence the event is rejected as pileup and does not appear in Fig. 3. Therefore, by gating on the appropriate region in the TAC spectrum of Fig. 3, we man-

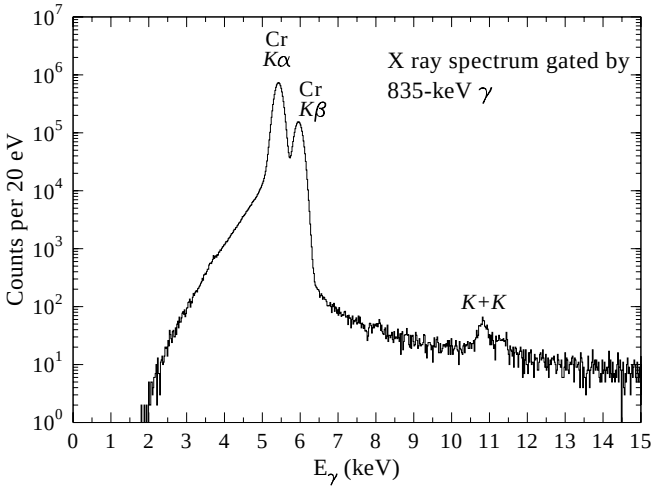

FIG. 4. X-ray spectrum recorded in the planar detector, in coincidence with the 835-keV line.

aged to bring down the effective pair-pileup resolution to 125 ns, which is at least a factor of 3 lower than the pair-pileup resolution of the amplifier.

III. DATA ANALYSIS

Figure 4 shows the x-ray spectrum gated by the 835-keV line and the above 2D gates, and Fig. 5 shows an expanded view of the region of the $K+K$ sums, together with a fit using the expected line shape. The region was fitted with the sum of seven peaks, superimposed on a quadratic background. Three peaks accounted for the accidental sum of two ''normal'' x rays: $K\alpha^N+K\alpha^N$, $K\alpha^N+K\beta^N$, and $K\beta^N+K\beta^N$, and four peaks accounted for the true sum of x rays produced from a double vacancy in the K shell: $K\alpha^S+K\alpha^H$, $K\alpha^H+K\beta^S$, $K\alpha^S+K\beta^H$, and $K\beta^H+K\beta^S$, where the superscripts H and S denote the hypersatellite and satellite x rays, respectively. A hypersatellite K x ray is emitted in filling the first of the two vacancies, and a satellite x ray is emitted in filling the second of the two vacancies. The hypersatellite x ray has a (considerably) higher energy than a satellite x ray, which in turn has a (slightly) higher energy than a normal x ray. A Gaussian shape plus an exponential on the low-energy side (to account for forward scattered x rays) was used for each of the peaks. The centroids and widths of the Gaussians were fixed to the values expected from the known energies and energy shifts of the normal, satellite, and hypersatellite peaks, and using an energy (and width) calibration based on Ge x-ray lines. The energy shifts of the hypersatellite x rays were taken from the measurements of Nagy and Schupp [5], while the energy shifts of the satellite x rays were calculated from a fit to the shifts calculated by Burch *et al.* [7]. Table I lists these shifts, as well as other relevant atomic parameters. Using the known relative intensities of the $K\alpha$ and $K\beta$ lines in Cr ($K\alpha/K_T=0.882$, $K\beta/K_T=0.118$ [8]) and the measured relative efficiency $\epsilon_{K\alpha}/\epsilon_{K\beta}=1.154$, one can determine the relative areas of the three normal peaks that arise from accidental summing, as well as the relative areas of the four hypersatellite-plus-satellite true sum peaks. Therefore, although the fit consisted of seven peaks, only five parameters were allowed to vary freely: the area of the $K\alpha^N+K\alpha^N$ peak, the area of the $K\alpha^S+K\alpha^H$ peak, and the three parameters of the quadratic background. Table II lists the energies, widths, and relative intensities of the seven peaks used in the fit, and Table III lists $N[\gamma\otimes(K\alpha^N+K\alpha^N)]$, the area of the accidental sum peak, $N[\gamma\otimes(K\alpha^S+K\alpha^H)]$, the area of the true sum-

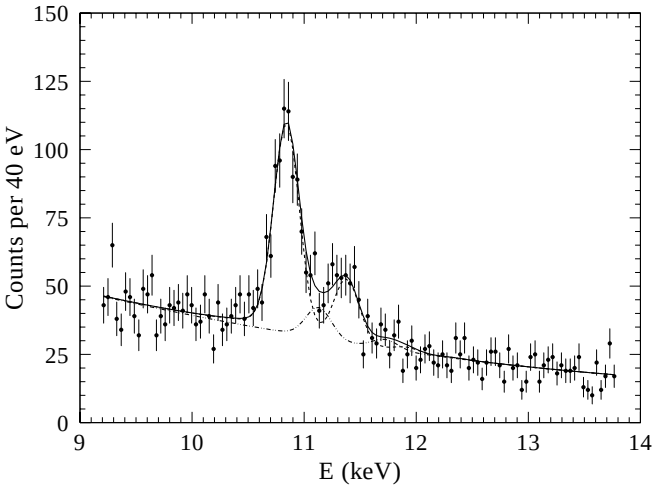

FIG. 5. The $K+K$ region of the x-ray spectrum gated by the 835-keV line. The solid curve shows the fit; the dashed curve shows the pileup component of the fit (K^N+K^N), while the dash-two-dotted curve shows the true (K^H+K^S) sum peaks.

TABLE I. Energy shifts of hypersatellite and satellite lines and atomic parameters relevant to the calculation of P_{KK}.

$\Delta K\alpha^H$ [a]	0.254 keV
$\Delta K\beta^H$ [a]	0.319 keV
$\Delta K\alpha^S$ [b]	0.033 keV
$\Delta K\beta^S$ [b]	0.087 keV
ω_K [c]	0.288
$K\alpha/K_T$ [d]	0.882
P_K [c]	0.8895

[a]Reference [5].
[b]Reference [7].
[c]Reference [11].
[d]Reference [8].

TABLE II. Centroids and relative intensities of the lines used in the fit to $\gamma\otimes(K+K)$ coincidences.

Component	E (keV)	FWHM (keV)	Relative intensity
$K\alpha^N+K\alpha^N$	10.824	0.266	1.000
$K\alpha^N+K\beta^N$	11.359	0.268	0.307
$K\beta^N+K\beta^N$	11.894	0.268	0.024
$K\alpha^S+K\alpha^H$	11.111	0.266	1.000
$K\alpha^H+K\beta^S$	11.700	0.268	0.154
$K\alpha^S+K\beta^H$	11.711	0.268	0.154
$K\beta^S+K\beta^H$	12.300	0.269	0.024

TABLE III. Experimental results.

$N[\gamma\otimes(K\alpha^N+K\alpha^N)]$	541 ± 31
$N[\gamma\otimes(K\alpha^S+K\alpha^H)]$	81^{+28}_{-18}
$N[\gamma\otimes K\alpha^N]$	2.622×10^7
$\epsilon_{K\alpha}$	5.25%
P_{KK}	$2.3^{+0.8}_{-0.5}\times10^{-4}$

coincidence peak, $N[\gamma\otimes K\alpha^N]$, the area of the normal γ-$K\alpha^N$ coincidence peak, the measured efficiencies, and the deduced value of P_{KK}.

The number of triple $\gamma\otimes(K\alpha^S+K\alpha^H)$ coincidences is related to P_{KK} by

$$N[\gamma\otimes(K\alpha^S+K\alpha^H)]=N_0P_KP_{KK}\epsilon_\gamma\left[\omega_K^H\left(\frac{K\alpha}{K_T}\right)^H\epsilon_{K\alpha}^H\right]\times\left[\omega_K^S\left(\frac{K\alpha}{K_T}\right)^S\epsilon_{K\alpha}^S\right], \quad (1)$$

where N_0 is the number of ^{54}Mn decays; P_K is the fraction of K-capture decays; ω_K^H and ω_K^S are the fluorescence yields for the Cr hypersatellite and satellite x rays, respectively; $(K\alpha/K_T)^H$ and $(K\alpha/K_T)^S$ are the fractions of hypersatellite and satellite $K\alpha$ x rays, respectively; and ϵ_γ, $\epsilon_{K\alpha}^H$, and $\epsilon_{K\alpha}^S$ are the detector efficiencies of the corresponding radiations. In the above, we have taken the radiative-decay fraction of the 835-keV level in ^{54}Cr to be unity, since its internal conversion coefficient $\alpha=2.5\times10^{-4}$ [9] is negligibly small. The number of recorded coincidences between the 835-keV γ ray and the normal $K\alpha^N$ x rays is given by

$$N[\gamma\otimes K\alpha^N]=N_0P_K\epsilon_\gamma\left[\omega_K^N\left(\frac{K\alpha}{K_T}\right)^N\epsilon_{K\alpha}^N\right]. \quad (2)$$

One can obtain P_{KK} by dividing Eq. (1) by Eq. (2) and rearranging. We simplify the result by noting that, to a very good approximation, $\epsilon_{K\alpha}^N=\epsilon_{K\alpha}^H=\epsilon_{K\alpha}^S$ and that $\omega_K^N\simeq\omega_K^H\simeq\omega_K^S$ [10]. Nagy and Schupp [5] found $(K\beta/K_T)^H=0.27$, i.e., $(K\alpha/K_T)^H=0.73$, whereas Lépy *et al.* [8] found $K\alpha/K_T=0.882$. However, neither the theoretical calculations of Chen, Crasemann, and Mark [10], nor any other measurements, found such a large difference between the fraction of $K\beta$ decay for single and double vacancies. Further, if such a large enhancement of $(K\beta/K_T)^H$ over $(K\beta/K_T)^N$ (a factor of 2.3) was to be used to deduce P_{KK} for ^{54}Fe [6], the resulting value (0.54×10^{-4}), extrapolated to the lower Z of ^{54}Mn, would be in even further disagreement with Nagy and Schupp's value of $P_{KK}=3.6\times10^{-4}$. Therefore we take, as we have done in our previous studies [1], $(K\alpha/K_T)^N=(K\alpha/K_T)^S=(K\alpha/K_T)^H$. With these simplifications P_{KK} can be obtained as

$$P_{KK}=\frac{N[\gamma\otimes(K\alpha^S+K\alpha^H)]}{N[\gamma\otimes K\alpha^N]}\times\frac{1}{\omega_K(K\alpha/K_T)\epsilon_{K\alpha}}. \quad (3)$$

The efficiency for x rays can be obtained in a self-consistent way from the data by dividing the number of 835-keV x-ray coincidences [given by Eq. (2)] by the number of 835-keV counts, given by

$$N[\gamma]=N_0\epsilon_\gamma \quad (4)$$

to obtain

$$\epsilon_{K\alpha}=\frac{N[\gamma\otimes K\alpha^N]}{N[\gamma]\omega_K(K\alpha/K_T)}. \quad (5)$$

In obtaining the efficiency, the data from the singles runs were used. The above procedure for obtaining the efficiency ensures that the absorption of the x rays in the source is taken properly into account.

We have examined the sensitivity of the deduced value of P_{KK} to the parameters used in the fit and to various other assumptions. First, we give an indication of the statistical significance of the extracted area of the $K\alpha^S+K\alpha^H$ peak; the χ^2 value at the minimum was 223.55 for 229 degrees of freedom, i.e., a reduced χ^2 of 0.976. The one-standard-deviation limits on $N[\gamma\otimes(K\alpha^S+K\alpha^H)]$ were extracted in the usual way: the area of the $K\alpha^S+K\alpha^H$ peak was held fixed at a given value and the other four parameters in the fit were allowed to vary freely to minimize χ^2; that value of χ^2 was recorded and then another value of the $K\alpha^S+K\alpha^H$ area was chosen and χ^2 was minimized again. A plot of the minimum χ^2 as a function of the $K\alpha^S+K\alpha^H$ peak area was made; the optimum value of the $K\alpha^S+K\alpha^H$ peak area is that at which χ^2 has its overall minimum value $(\chi^2_{\min})$ and the one-standard-deviation values are those at which $\chi^2=\chi^2_{\min}+1$. It should be noted that the χ^2 value obtained assuming no hypersatellite peaks is 14.8 units above $\chi^2_{\min}$; thus the probability that the hypersatellite peaks are statistically significant is 99.9877%.

The sensitivity of the $K\alpha^S+K\alpha^H$ peak area to the assumed energy shift of the hypersatellite peak was examined by performing fits with $\Delta K\alpha^H$ and $\Delta K\beta^H$ varied by up to ±40 eV; this variation is about twice the experimental uncertainty of 18 and 22 eV given by Nagy and Schupp [5] for the respective Δ's. The resulting $N[\gamma\otimes(K\alpha^S+K\alpha^H)]$ changed by at most six counts, which is small compared to our quoted statistical uncertainty of $^{+28}_{-18}$.

As mentioned earlier, the centroids and widths of the peaks were based on an energy (and width) calibration obtained from Cr and Ge x rays. The Cr x rays are those obtained in coincidence with the 835-keV line (Fig. 4); the Ge x-rays were obtained by gating the signal in the coaxial Ge detector on the 835$-$Ge(K) escape peak, with the escaping Ge K x rays detected in coincidence by the planar detector. The Ge x rays are useful for calibration not only because their energies ($K\alpha_1=9.886$, $K\alpha_2=9.855$, $K\beta_{1,3}=10.980$, and $K\beta_2=11.101$ keV) are very close to those of the Cr $(K+K)$ sum peaks (Table II), but also because they are collected along with the Cr x rays throughout the measurement and hence their widths and centroids reflect the average over the total collection time of the experiment. A linear least squares fit of energy versus centroid was used for the energy

calibration, and a linear fit of the variance σ^2 of the Gaussian versus peak energy was used for the width calibration. The statistical uncertainty in the Ge $K\alpha$ centroid was 1.0 eV, and that of its σ was 1.6 eV [full width at half maximum (FWHM) $=2.354\sigma$]. To test the sensitivity of our results to the (slightly) extrapolated widths that were used, we performed fits in which the widths (σ's of the Gaussians) were varied by ± 4 eV from those corresponding to the central values listed in Table II, and found that $N[\gamma\otimes(K\alpha^S+K\alpha^H)]$ changed by at most six counts.

A legitimate concern that might be raised concerning the assumed centroids and widths of the pileup K^N+K^N peaks is the following. The calibrations are based on the energy of single x rays entering the detector, while the pileup peaks are the result of two x rays entering the detector at different times, within the time resolution of the pileup rejection gates (software and hardware); because of the finite charge collection time of the amplifier the resulting pileup signal could, in principle, have a slightly smaller amplitude and potentially larger variance than that of a single x ray (or two truly coincident x rays) with the summed energy. To address this concern, we performed fits on the spectra obtained by gating the TAC signal vs energy 2D spectrum (Fig. 3) on the accidentals region (below TAC channel 240 or above TAC channel 280). In these accidentals spectra the time separation between the pileup pulses is larger than that in the true-time-gated spectra and hence the centroid of the K^N+K^N peaks should be lower. The fits to the accidentals spectra with the centroids and widths of both the $K\alpha^N+K\alpha^N$ and $K\alpha^N+K\beta^N$ peaks, being allowed to vary freely gave centroids that are, respectively, 30 ± 7 eV and 31 ± 14 eV below the fixed centroids used in the main fits, and σ's that are 1 ± 5 eV less. As argued above, the time separation between the pileup pulses in the true-time-gated spectrum should be less than that in the accidentals spectra and hence the shift in the centroid of the pileup peaks should be, if anything, less than the 30 eV found for the accidentals. Nevertheless, to see how such a shift would affect our results, we conducted a fit to the true-time-gated spectrum with the centroids and widths fixed to the values obtained from the fits to the accidentals spectra. The result was 100 ± 24 for the $K\alpha^S+K\alpha^H$ peak area, which is still less than one standard deviation from our adopted result (Table III). Further, χ^2 for this fit was 231.16 for 229 degrees of freedom, clearly worse than the value of 223.55 obtained before. A fit to the true-time-gated spectrum in which the centroids of the $K\alpha^N+K\alpha^N$ and $K\alpha^N+K\beta^N$ pileup peaks were allowed to vary freely (but those of the true hypersatellite-plus-satellite sum peaks held fixed at the calibration values) was also made; the centroids found for the $K\alpha^N+K\alpha^N$ and $K\alpha^N+K\beta^N$ peaks were, respectively, 6 ± 8.8 and 11 ± 24 eV below the fixed values used in the main fit (Table II) and the $K\alpha^S+K\alpha^H$ peak area was 83 ± 30. Clearly, these values are consistent with those obtained from the main fit with the centroids and widths fixed from the calibrations.

To test whether the $K\alpha^S+K\alpha^H$ peak area was being unduly affected by any inadequacy in the assumed peak shape, we performed fits to the accidentals spectra obtained above using exactly the same number of parameters as was used in true-time-gated spectrum, i.e., allowing for a hypersatellite-plus-satellite component with a free amplitude. The area of the $K\alpha^S+K\alpha^H$ peak in the accidentals should be negligible, unless it was compensating for a bad peak shape for the K^N+K^N pileup peaks. The results were $K\alpha^N+K\alpha^N$ peak area is 445 ± 20, $K\alpha^S+K\alpha^H$ peak area is 12 ± 14, for a spectrum gated on the accidentals region below the true-time locus, and $K\alpha^N+K\alpha^N$ peak area is 460 ± 26, $K\alpha^S+K\alpha^H$ peak area is -10 ± 23, for a spectrum gated on the accidentals region above the true-time locus. The small value obtained for the $K\alpha^S+K\alpha^H$ peak area in these fits (consistent with zero within the statistical uncertainty) bolsters our confidence in the correctness of the peak shape used.

As a final test of the spectral shape used in the fit, we conducted fits in which the size of the fitted region was reduced by up to 3.0 keV; this reduced the number of degrees of freedom from 229 to 122, with all of the reduction coming from the background channels. If the peak yields were in any way compensating for curvature in the background that was not being adequately represented by the quadratic form used, then one would expect this yield to change in a substantial way as the size of the background region varied. However, these fits gave the same peak areas as before (with, as expected, a larger statistical uncertainty). This test, together with the perfectly acceptable χ^2 value obtained for the main fit, convinces us that a quadratic is sufficient to describe the shape of the background over the relatively small (4.6 keV) fitting region. The origin of this continuum background is discussed below.

To test for the presence of peaks in the fitted region that are not associated with the 835-keV peak, but with the continuum underneath it, we performed fits on the spectra obtained by gating the signal in the coaxial Ge detector on the continuum region above the 835-keV peak (Fig. 1). This region is dominated by 835-plus-835 Compton pileup and, to a lesser extent, by Comptons of the 1173-keV and 1332-keV lines due to the ^{60}Co contaminant in the source. For a gate of the same width used on the 835-keV peak, the yields were 2.4 ± 4.7 counts for the area of the $K\alpha^N+K\alpha^N$ peak, and 1.3 ± 4.6 counts for the area of the $K\alpha^S+K\alpha^H$ peak. Clearly, these yields are negligible compared to those obtained in coincidence with the 835-keV line and, again, give us confidence that the peaks in the main spectrum are being correctly interpreted.

By comparing the continuum yield in the region of the $K+K$ peaks in the spectra gated on the accidentals region and that gated above the 835-keV line, to the continuum yield in the true-time-gated spectrum, we conclude that approximately 20% of the continuum in the true-time-gated spectrum comes from accidental (835-835)-keV Compton coincidences and (835-plus-835)-keV pileup. That is, about 80% of the continuum is due to real coincidences of γ rays with the 835-keV line. Where does this continuum come from? A rough estimate of its yield indicates that this continuum is compatible with internal bremsstrahlung (IB) accompanying the EC decay of ^{54}Mn [12]. The IB itself should not have a structure in the energy region of the fit, and is adequately described by a quadratic over the limited region of the fit; however, the IB could, in principle, lead to x rays

in that energy region through the fluorescence of the material surrounding the detector. Indeed, we find that the small but statistically significant peak at 8.03 keV, somewhat visible in Fig. 4, is predominantly in coincidence with the 835-keV peak, and is most likely due to the fluoresence by the IB of the substantial amount of copper in the graded shield surrounding the detectors. The only elements having K x rays with energies that are close to the Cr $K+K$ sum energy are Ge, As, and Se. While there is clearly a substantial amount of Ge in the vicinity of the planar detector, namely the coaxial Ge detector, only a negligible amount of Ge x rays could come from that detector when the signal in it is gated on the 835-keV line. If an IB γ ray enters the coaxial detector simultaneously with the 835-keV γ ray line, then the summed signal will throw the event out of the 835-keV gate. Only the sum of an IB photon with a Compton-scattered 835-keV γ ray could fall in the 835-keV gate; but in that case one would expect as many Ge escape x rays with a spectrum gated on the continuum region just above the 835-keV line. As mentioned above, such a spectrum was obtained and analyzed, and was found to contain no peaks in that region. The best proof, though, that Ge x rays are not produced with the 835-keV gate is that the coincidence spectrum in Fig. 5 does not show the Ge $K\alpha$ x ray expected at 9.9 keV. We note that only the Ge $K\beta$ x ray ($\approx$11 keV) would be in the $K+K$ peak area, and that its intensity would be about 13% of any potential Ge $K\alpha$ peak at 9.9 keV. That leaves the possibility of As and Se K x rays. The detectors were surrounded by a massive graded shield consisting of Pb, Cu, and Al and, to our knowledge, there were no As or Se compounds present. These elements have a much smaller natural abundance than Cu and Al and different chemistries, and hence it would be a surprise to us if they were present in a significant amount as contaminants in either. These elements are also not found in the detector components in significant amounts. If L x rays of fluoresced elements were contaminating the Cr $K+K$ region, then the corresponding K x rays of those elements would have been observed (the gain of the planar Ge detector allowed energies up to 150 keV to be observed in the spectrum). No x-ray lines above the Cr $K+K$ region were visible in the 835-keV-gated spectrum.

As mentioned previously, we have assumed $(K\alpha/K_T)^H=(K\alpha/K_T)^N$, consistent with all the previous analyses of P_{KK} measurements and with the theoretical expectations. However, to find out to what degree our deduced value of P_{KK} depends on that assumption, we conducted a fit in which the relative intensities of the various satellite-plus-hypersatellite peaks were fixed at values deduced by using $(K\beta/K_T)^H=0.27$, i.e., the value quoted by Nagy and Schupp [5]. In that case, we find $P_{KK}=(2.4^{+0.8}_{-0.5})\times10^{-4}$, a value virtually identical to that of our adopted result (Table III). The χ^2 value obtained with $(K\beta/K_T)^H=0.27$ is 224.47 for 229 degrees of freedom, which is slightly worse than the value of 223.55 obtained with our assumption of $(K\alpha/K_T)^H=(K\alpha/K_T)^N=0.118$.

Finally, we consider the assumption of the near equality of the normal, hypersatellite, and satellite fluorescence yields ($\omega_K^N\simeq\omega_K^H\simeq\omega_K^S$), an assumption based on theoretical calculations [10]. The experimentally measured quantities, namely the peak areas, are not affected in any way by any assumptions made about the fluorescence yields and hence there is no way to test that assumption experimentally in our setup. To our knowledge, all the measurements of P_{KK} to date have made that assumption; in particular the measurements of P_{KK} for ^{65}Zn [4], ^{54}Mn [5], and ^{55}Fe [6] have made use of that assumption. To the extent that the current experiment is being conducted to verify the previously measured value for ^{54}Mn, in an attempt to resolve the seeming descrepancy between its value and that of the neighboring atom ^{55}Fe, we should use the same assumptions on the fluorescence yields as used before. That is, should the ratio ω^H/ω^N be found in some future experiment to be, contrary to the theoretical expectations, substantially different from unity, then one would probably still expect the ratio to vary smoothly with Z and hence for the previous seeming descrepancy between ^{54}Mn and ^{55}Fe to remain. Should a future experiment find the normal, hypersatellite, and satellite fluorescence yields to be different from each other, then one can simply obtain the ''correct'' P_{KK} by multiplying our reported value by $(\omega_K^N/\omega_K^H)\times(\omega_K^N/\omega_K^S)$.

IV. RESULTS AND DISCUSSION

The result of the present experiment for P_{KK} is $(2.3^{+0.8}_{-0.5})\times10^{-4}$. This result is about 1.6 standard deviations lower than the value of $(3.6\pm0.3)\times10^{-4}$ measured by Nagy and Schupp [5]. Assuming a $1/Z^2$ dependence for P_{KK}, which is the dependence predicted by the Primakoff-Porter theory [13], the value of P_{KK} extrapolated from the measurement of Campbell *et al.* [6] for ^{55}Fe is $(1.4\pm0.2)\times10^{-4}$, which is 1.8 standard deviations below our results. Thus our result falls in between Nagy and Schupp's result and that extrapolated from the result of Campbell *et al.* and disagrees with both, but not at a very high level of statistical significance. Because ours is a triple-coincidence experiment, while Nagy and Schupp's is a double-coincidence experiment, and that of Campbell *et al.* is a singles experiment, our statistical error is larger than these previous experiments. It is unlikely that we would be able to reduce the statistical error on our measurement significantly without running for a substantially longer time (the data in this experiment took 4 months to collect), or obtaining detectors with much larger efficiency. Although our statistical error is larger than that of these two previous measurements, requiring a coincidence with the 835-keV γ ray ensures that the x rays we observe come from the decay of ^{54}Mn and not from some small contaminant in the source or from the fluorescing of the source or adjacent material by the 835-keV γ ray. In summary, while our result does not conclusively support or reject one or the other of the two previous P_{KK} values for ^{54}Mn, it does seem to indicate that the value is not as far above the smooth trend of the neighboring P_{KK}'s as suggested by the measurement of Nagy and Schupp [5].

As noted in the Introduction, there is also a divergence between the two leading theoretical approaches to the calculation of P_{KK}, the semirelativistic propagator (SRP) method of Intemann [2] and the self-consistent-field (SCF) method of Law and Suzuki [3]. Except for the decays with low Q

values [1], where both theories are on the lower side of the measurements, the two theories bracket most of the existing experimental data, with the SCF theory being on the higher side and the SRP theory being on the lower side. For ^{54}Mn, the SRP calculation predicts $P_{KK}=1.125\times10^{-4}$, in closer agreement with the result of Campbell *et al.*, while the SCF calculation predicts $P_{KK}=2.43\times10^{-4}$, in closer agreement with our result.

ACKNOWLEDGMENT

This work was supported by U.S. DOE Grant No. DE-FG02-96ER40955.

[1] See, for example, M.M. Hindi and R.L. Kozub, Phys. Rev. C **45**, 1070 (1992), and references therein; M.M. Hindi, R.L. Kozub, H.J. Nagy, and G. Schupp, *ibid.* **44**, 2237 (1991).

[2] R.L. Intemann, Phys. Rev. C **31**, 1961 (1985).

[3] J. Law and Akira Suzuki, Phys. Rev. C **25**, 514 (1982).

[4] H.J. Nagy and G. Schupp, Phys. Rev. C **27**, 2887 (1983).

[5] H.J. Nagy and G. Schupp, Phys. Rev. C **30**, 2031 (1984).

[6] J.L. Campbell, J.A. Maxwell, and W.J. Teesdale, Phys. Rev. C **43**, 1656 (1991).

[7] D. Burch, L. Wilets, and W.E. Meyerhof, Phys. Rev. A **9**, 1007 (1974).

[8] M.C. Lépy, J. Plagnard, and J. Morel, Nucl. Instrum. Methods Phys. Res. A **339**, 241 (1994).

[9] *Table of Isotopes*, edited by C.M. Lederer and Virginia S. Shirley, 7th ed. (Wiley, New York, 1978).

[10] M.H. Chen, B. Crasemann, and H. Mark, Phys. Rev. A **25**, 391 (1982).

[11] *Table of Isotopes*, edited by R.B. Firestone, 8th ed. (Wiley, New York, 1996).

[12] M.M. Hindi, R.-M. Larimer, E.B. Norman, and G.A. Rech, Phys. Rev. C **61**, 055501 (2000), and references therein.

[13] H. Primakoff and F.T. Porter, Phys. Rev. **89**, 930 (1953).